Available online at www.sciencedirect.com
ScienceDirect
Earth and Planetary Science Letters 261 (2007) 517–533
EPSL
www.elsevier.com/locate/epsl

U-series isotope and geodynamic constraints on mantle melting processes beneath the Newer Volcanic Province in South Australia

Zoe Demidjuk [a,1], Simon Turner [a,*], Mike Sandiford [b], Rhiannon George [a], John Foden [c], Mike Etheridge [a]

[a] GEMOC, Department of Earth and Planetary Sciences, Macquarie University, Sydney, NSW 2109, Australia
[b] School of Earth Sciences, University of Melbourne, VIC 3010, Australia
[c] School of Earth and Environmental Sciences, University of Adelaide, Adelaide, SA 5005, Australia

Received 25 July 2006; received in revised form 13 February 2007; accepted 10 July 2007
Available online 17 July 2007
Editor: C.P. Jaupart

Abstract

Young (<5 kyr) olivine- and clinopyroxene-phyric *ne*-hawaiites from Mounts Gambier and Schank in the Newer Volcanic Province in South Australia have been analysed for major and trace elements as well as for Sr and Nd isotopes and ^{238}U–^{230}Th disequilibria in order to constrain the mantle melting processes responsible for their origin. The rocks are relatively primitive (6.9–9.1% MgO), incompatible trace element-enriched alkali basalts with $^{87}Sr/^{86}Sr = 0.70398–0.70415$ and $^{143}Nd/^{144}Nd = 0.51280–0.51271$. Trace element modelling suggests that they reflect 3–6% partial melting in the presence of 2–8% residual garnet. Trends towards low K/K* are accompanied by decreasing $^{87}Sr/^{86}Sr$ and provide evidence for the involvement of hydrous phases during melting. ^{230}Th excesses of 12–57% cannot be simulated by batch melting of the lithosphere and instead require dynamic melting models. It is argued that the distinction between continental basalts bearing significant U–Th disequilibria and those in secular equilibrium reflects dynamic melting in upwelling asthenosphere, rather than static batch melting within the lithosphere or the presence or absence of residual garnet. Upwelling rates are estimated at ~1.5 cm/yr. A subdued, localised topographic uplift associated with the magmatism suggests that any upwelling is more likely associated with a secondary mode localised to the upper mantle, rather than a broad zone of deeply-sourced (plume) upwelling. Upper mantle, 'edge-driven' convection is consistent with seismic tomographic and anisotropy studies that imply rapid differential motion of variable thickness Australian lithosphere and the underlying asthenosphere. In this scenario, melting is linked to a significant contribution from hydrous mantle that is envisaged as resulting either from convective entrainment of lithosphere along the trailing edge of a lithospheric keel, or inherited variability in the asthenosphere.

Keywords: alkali basalt; geochemistry; U–Th isotopes; intraplate magmatism; edge-driven convection; South Australia

1. Introduction

Spatially and often volumetrically extensive, basaltic, intraplate magmatism is frequently attributed to partial melting within upwelling mantle plumes although the details of the melting processes are not always well

* Corresponding author.
E-mail address: sturner@els.mq.edu.au (S. Turner).
[1] Present address: SRK Consulting Ltd. Level 6, 44 Market Street, Sydney NSW 2000, Australia.

0012-821X/$ - see front matter © 2007 Elsevier B.V. All rights reserved.
doi:10.1016/j.epsl.2007.07.006

understood (see Mahoney and Coffin, 1997, for a review). In the oceans, U-series disequilibria have provided important constraints on the porosity and upwelling rate of the melting regions of mantle plumes (see Bourdon and Sims, 2003, for a review) but significantly less information is yet available for basaltic provinces emplaced on the continents (Reid, 1995; Asmerom and Edwards, 1995; Reid and Ramos, 1996; Huang et al., 1997; Asmerom, 1999; Asmerom et al., 2000). In this setting there is considerable debate as to whether "non-asthenospheric" trace element and/or isotope signatures are intrinsic to putative plumes or alternatively whether such signatures are derived from the subcontinental lithospheric mantle or reflect crustal contamination (see Farmer, 2004, for a review). Furthermore, King and Anderson (1998) have argued that, in some instances, melting might result from convection driven by plate edge effects rather than requiring the presence of a deep-seated mantle plume. These debates are especially relevant to the well documented Newer Volcanic Province of southeastern Australia where a long-standing problem has been to explain why mantle melting occurred in the absence of extension or any convincing evidence for the presence of a mantle plume. The youngest eruptives in the Newer Volcanic Province are primitive and amenable to U–Th disequilibria measurements and thus afford the opportunity to gain fresh insights into some of these substantive issues.

2. Background and previous work

The Newer Volcanic Province (Fig. 1) represents the most recent stage of a long-lived, intermittent, low-volume magmatic province erupted across south-eastern Australia between 190 Ma and a few ka (Price et al., 2003). Magmatic activity is concentrated between 0–5 Ma, distinguishing it from the "Older" volcanics where activity peaked in the early Miocene (~22 Ma) and Eocene (39–50 Ma). The Newer Volcanic Province covers an area of ~15 000 km^2 but, with typical thicknesses of ≤60 m, the estimated total volume

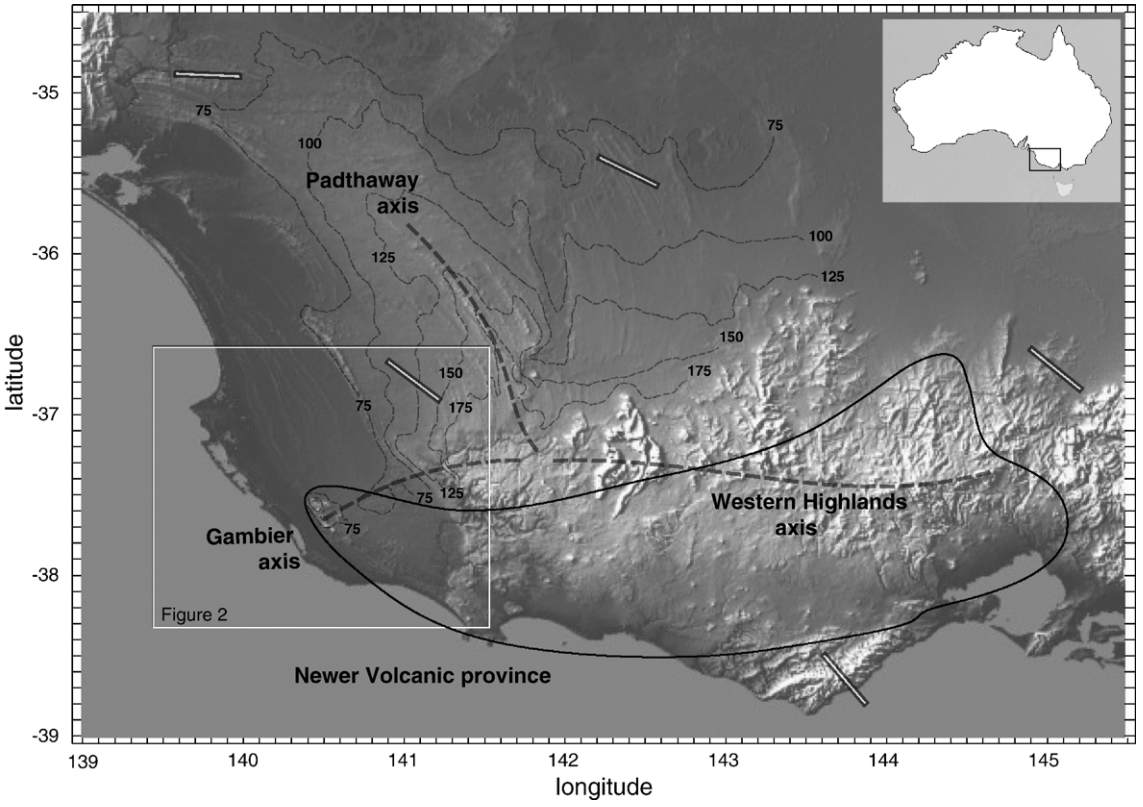

Fig. 1. Digital topography (SRTM 3 arcsecond) of SE South Australia and western Victoria, showing distribution of the Newer Volcanic Province and the main axes of Neogene uplift. Contours show elevation of the Pliocene strand plain of the Murray Basin showing ~200 m of uplift along the Padthaway axis (see Wallace et al., 2005, in press). Bars show regional trends of the maximum compressive stress (see Sandiford et al., 2004).

(20 000 km^3) is quite small (e.g. Johnson et al., 1989; Price et al., 2003) compared to many other continental basaltic provinces. The extended duration, small volume and lack of any single, simple age progression (Sutherland, 2003) means that the applicability of mantle plume models is not straightforward. Erupted products have been divided into the "Plains" and "Cones" series by Price et al. (1997) and the geochemistry of the lavas and their entrained mantle xenoliths in Victoria has been investigated in a number of studies including the pioneering petrological work of Frey et al. (1978). Many of these have recognised both an enriched lithospheric mantle component and component with affinities to ocean island basalts (OIB) (e.g. Price et al., 1997; Handler et al., 1997; McDonough et al., 1985; McDonough and McCulloch, 1987; Griffin et al., 1988; O'Reilly and Griffin, 1988; Zhang et al., 2001; Foden et al., 2002; Paul et al., 2005). However, there has been debate over which of these components dominates the Plains versus Cones series (e.g. McDonough and McCulloch, 1987; Price et al., 1997; McBride et al., 2001). Crucially, the role of upwelling asthenosphere and whether the OIB component may reside here has not yet been resolved, irrespective of whether or not this may take the form of a mantle plume (e.g. Paul et al., 2005).

In South Australia, the youngest components of the Newer Volcanics are manifest as ~15 Quaternary centres along the Mount Burr Range and as two Holocene centres at Mounts Gambier and Schank (Fig. 2). The latter two centres are mainly maars or scoria cone-type volcanoes and represent the youngest volcanic centres on the Australian continent and yet surprisingly little geochemical data has yet been published from these rocks (McDonough and McCulloch, 1987; Foden et al., 2002). Consequently, we have analysed major and trace elements and Sr and Nd isotopes as well as ^{238}U–^{230}Th disequilibria in samples from Mounts Gambier and Schank in order to better document these centres and to determine whether or not the melting that produced these rocks occurred in upwelling asthenospheric mantle or in static lithospheric mantle. We begin with an assessment of the age, volume, duration and topographic response to magmatism in the South Australian sector of the Newer Volcanic Province.

3. Age, volume and topographic response to basaltic magmatism

The Newer Volcanics overlie the Late Eocene to Mid-Miocene Gambier Limestone placing a maximum age on their emplacement. In the Mount Burr region the volcanics are overlain by the Bridgewater Formation which is Pleistocene to Recent in age. Combining these constraints with palynologial data, Sheard (Sheard, 1978, 1995) has estimated the Mount Burr Range volcanics to have erupted around 1 Myr to 20,000 years BP. In contrast, at Mounts Gambier and Schank, the volcanics overlie the Bridgewater Formation and ^{14}C ages (1410 and 4830 yrs BP) and palaeomagnetic data suggest that they were erupted less than 5 kyr ago (Barbetti and Sheard, 1981; Blackburn et al., 1982).

The volume of the South Australian Newer Volcanic Province is constrained by known aerial outcrop extent, drill hole data and associated magnetic anomalies. The volcanics have an outcrop aerial extent of 110 km^2 with a thickness reaching up to 160 m (e.g. Sheard, 1978, 1995). Using drill-hole data, Demidjuk (2005) estimated that subsurface continuations give a total aerial real extent of 217 km^2 and a minimum volume of 3 km^3. Allowing for partial erosion of older sequences in the Mount Burr Range suggests the original volume of the erupted volcanics may have been as much as ~5 km^3. Regional and high-resolution airborne magnetic surveys reveal a series of moderate wavelength highs as well as shorter wavelength magnetic anomalies coincident with the outcropping volcanics (Teasdale, 2004) indicative of shallow intrusives beneath the volcanics. Detailed magnetic field surveys and palaeomagnetic analysis by Demidjuk (2005) indicate that the subsurface rocks either have a different age to the surface volcanics or they have different magnetic properties, indicating that they represent either older basalt flow(s) or shallow intrusions. In either case the estimated volume for the modelled bodies is considerably less than the estimated volume of the surface volcanics, and the total volume is estimated to be no greater than 10 km^3 and probably more like 5 km^3.

The South Australian volcanics are associated with a pattern of subdued regional uplift centred around the Mt Burr Range, exquisitely evidenced by uplifted Quaternary shoreline ridges along the Gambier coastal plain (Figs. 1 and 2). The deflection of these Quaternary highstand ridge systems records an accumulated uplift of up to 60 m over the last 780 kyr giving a regional uplift rate of some 75 m/Myr. Resolution of the uplift history prior to the Brunes–Matyama transition is much poorer, although older shoreline features of early Quaternary or late Pliocene age extend to elevations of up to 200 m in western Victoria (Sandiford, 2003; Wallace et al., 2005, in press), implying that the modern regime reflects a regional doming that has been operative over most of the Quaternary. Intriguingly, uplift along the South Australian–Victorian border

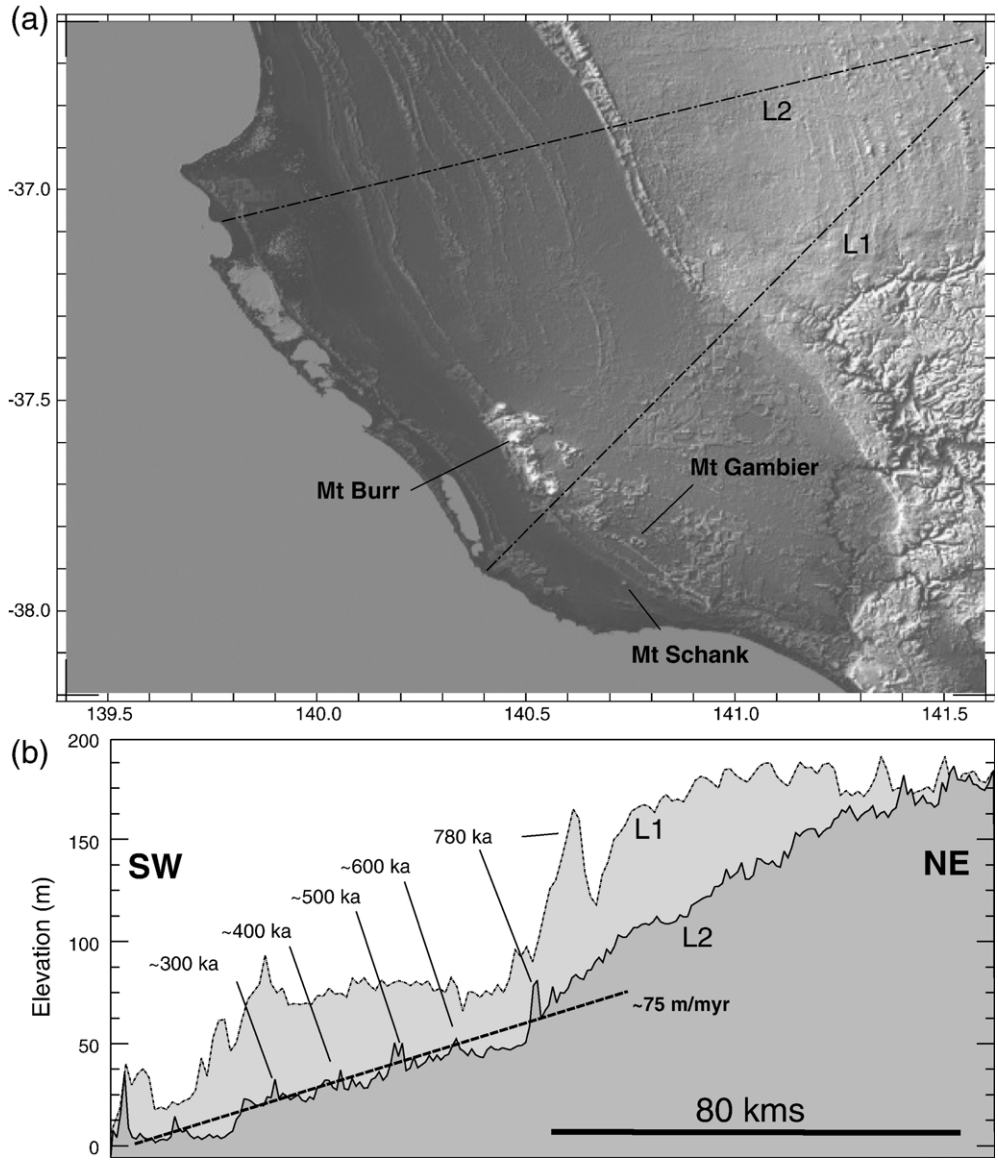

Fig. 2. (a) Detailed topography of the Gambier plains showing stranded Quaternary beach ridges wrapping around the Gambier volcanic province. Age constraints show beach ridges formed during high sea stands, and indicate an uplift of ~75 m/myr has operated for the last several million years. (b) Topographic profiles across the Pliocene–Quaternary strand plain. Ages of the high sea stand shoreline ridges from (Belperio, 1995). The volcanic region (profile L1) is typically elevated above the adjacent strandplain (profile L2) by some 30–50 m.

contributed to the damming of the Murray River to form a huge inland palaeo-lake system, termed Lake Bungunia, at about 3.5 Ma (Wallace et al., 2005). The present E–W branch of the Murray River follows the depocentre of this ancient lake system which seems to have been a site of persistent gentle subsidence through much of the Cenozoic.

This elongated zone of domal uplift can be traced ~400 km east across much of the western Victorian highlands where it corresponds broadly with the northern parts of the Newer Volcanic Province, and where commencement of uplift seems to date back at least to the Oligocene (Holdgate et al., 2006). To the northeast of the Gambier Volcanics, the uplift appears to bifurcate into two arms — the Padthaway and Gambier axes. The characteristic wavelength of each of these arms is on the order of 100 km. Neither is associated with any significant crustal faulting suggesting the

topographic response is associated with a lithospheric doming or flexural response related to infra- or sub-lithospheric loading, or buckling in response to in-plane stress. The pattern of *in-situ* stress in south-east Australia shows regional NW–SE compression aligned almost parallel to the Padthaway axis (Fig. 1, Sandiford et al., 2004), thus precluding a buckling response to *in-situ* stress for this feature.

4. Analytical techniques

The samples analysed here form part of a larger collection from Song (1994) that were taken from the upper sequences at Mounts Gambier and at Mount Shank from the main lava field which is overlain by the volcanic cone. Major and trace elements were determined using standard techniques (Potts et al., 1984; Eggins et al., 1997) using a Phillips® PW1480 XRF at the University of Adelaide and an Agilent® 7500 ICP-MS at Macquarie University, respectively. The isotopic compositions of Nd and Sr were determined at the University of Adelaide by thermal ionisation mass spectrometry using a Finnigan MAT® 262 instrument. Analyses were performed on ~200 mg of powdered sample that was dissolved using HF–HNO_3 in a heated teflon pressure bomb. The product was converted to chloride using 6 N HCl. Sr and REE fractions were separated using a cationic column after which Sm and Nd were separated on a HDEHP column. The Sr and Nd fractions were loaded onto single Ta and double Ta–Re filaments, respectively, and analysed in static mode. Sr and Nd isotopes were corrected for mass fractionation by normalising $^{86}Sr/^{88}Sr$ to 0.1194 and $^{146}Nd/^{144}Nd$ to 0.7219, respectively. Blanks measured during these analyses were 370 pg of Nd and Sm and 1.2 ng of Sr. Reproducibility was monitored by full procedural analysis of a Tasmanian Basalt in-house standard. Values obtained for the NSB 987 and La Jolla solution standards during the course of the analytical program were 0.710183±37 and 0.511846±30, respectively.

U and Th concentrations and isotope ratios were determined on samples that were spiked with a ^{226}U–^{229}Th tracer and dissolved using an HF–HNO_3–HCl mix in heated teflon pressure bombs. The product was converted to chloride using 6 N HCl and then 6 N HCl saturated with boric acid to remove residual fluorides. The final product was converted to nitrate using 14 N HNO_3 and finally taken up in 7 N HNO_3. U and Th purification was achieved via a single pass through a 4 ml anionic resin column using 7 N HNO_3, 6 N HCl and 0.2 N HNO_3 as elutants. Concentrations and isotope ratios were measured in dynamic mode on a Nu Instruments® MC-ICP-MS at Macquarie University. ^{238}U and ^{235}U were analysed on Faraday cups, using the $^{238}U/^{235}U$ ratio to determine the mass bias, assuming $^{238}U/^{235}U = 137.88$, whilst ^{236}U and ^{234}U were alternately collected in the IC0 ion counter which is equipped with a deceleration lens. The IC0 gain was determined during interspersed dynamic analyses of CRM145 assuming a $^{234}U/^{238}U$ ratio of 5.286×10^{-5} (Cheng et al., 2000). Th isotopes were also measured dynamically with ^{232}Th in Faraday cups and ^{230}Th and ^{229}Th alternating on IC0. The mass bias and gain for these measurements was taken in the first instance from measurements of CRM145. Differences in the mass bias for U and Th were then determined by interspersed analyses of the Th′U′ solution standard. Accuracy (<0.3%) and precision (<0.1%) were assessed by regular analyses of the U010 and ThA solution standards and of the secular equilibrium rock standard TML-3 (see Dosseto et al., 2006).

For two samples, Ra was taken from the first elution from the anionic column and converted to chloride using 6 N HCl. This was then loaded in 3 N HCl onto an 8 ml cationic column and eluted using 3.75 M HNO_3 and the process repeated on a scaled-down 0.6 ml column. Ra and Ba were then chromatographically separated using ElChrom® Sr-spec resin™ and 3 N HNO_3 as elutant in a 150 µl procedure. Samples were loaded onto degassed Re filaments using a Ta-HF-H_3PO_4 activator solution and $^{228}Ra/^{226}Ra$ ratios were measured to a precision typically ~0.5% in dynamic ion counting mode on a Thermo-Finnigan Triton® TIMS at Macquarie University. Accuracy was assessed via replicate analyses of TML-3 which yielded $^{226}Ra = 3534$ fg/g and $(^{226}Ra/^{230}Th) = 1.002 \pm 0.008$ ($n = 5$). Activity ratios (denoted by brackets) were calculated using the half lives compiled in (Bourdon et al., 2003).

5. Results

The lavas are olivine-and clinopyroxene-phyric (8–25%) undersaturated, *ne*-hawaiites with a microcrystalline groundmass containing olivine, clinopyroxene and plagioclase (Song, 1994). Thermobarometry using the method of Putrika et al. (1996) suggests that the clinopyroxene phenocrysts equilibrated with their groundmass at 1105–1224 °C at pressures of 0.2–0.3 GPa (Demidjuk, 2005). Some of the lavas at Mount Gambier contain numerous spinel–lherzolite xenoliths indicating that the magmas travelled quickly through the crust and so probably did not interact significantly with it en-route to the surface. The analytical results

Table 1
Representative analyses of alkali basalts from Mount Gambier and Mount Schank

Sample No.	GA-1	GA-3	GA-4	GA-7	GA-8	GA-9	SH-1	SH-2	SH-3	SH-4	SH-5
SiO_2 (wt.%)	48.55	47.25	49.28	48.56	49.63	47.41	47.30	46.82	47.28	47.23	47.14
TiO_2	2.43	2.43	2.18	2.30	2.28	2.33	3.06	3.07	3.10	3.03	3.09
Al_2O_3	14.14	13.55	13.47	13.37	13.50	13.16	14.41	14.36	14.48	14.46	14.48
Fe_2O_3	12.16	12.00	12.25	12.46	12.41	12.16	12.38	12.25	12.39	12.37	12.29
MnO	0.16	0.17	0.16	0.16	0.16	0.16	0.16	0.16	0.16	0.16	0.16
MgO	7.78	8.51	9.07	8.80	8.19	8.55	6.89	6.92	6.99	6.96	6.89
CaO	8.53	8.38	8.88	9.33	9.05	9.47	7.43	7.44	7.40	7.42	7.42
Na_2O	3.99	4.79	3.59	3.57	3.79	3.85	4.60	4.56	4.78	4.74	4.76
K_2O	1.86	2.53	1.46	1.49	1.54	1.66	3.04	2.98	3.01	3.01	3.00
P_2O_5	0.62	0.86	0.47	0.54	0.50	0.56	1.06	1.05	1.07	1.05	1.06
SO_3	0.01	0.01	0.00	0.01	0.03	0.2	0.17	0.09	0.02	0.06	0.03
Total	99.75	100.03	100.11	100.02	100.49	99.94	100.89	99.78	100.03	99.92	99.65
Li (ppm)	–	7.08	5.71	7.40	5.74	–	7.31	7.41	7.64	7.37	7.40
Be	–	2.98	1.66	3.05	1.65	–	3.05	3.15	3.09	3.12	3.13
Sc	38.3	18.8	21.5	15.3	20.6	24.8	15.2	15.7	15.5	15.9	15.6
V	333	176	176	166	176	363	163	166	164	168	166
Cr	235	297	282	146	260	141	140	143	142	145	142
Co	125.8	47.4	56.2	43.2	53.6	147.1	48.9	45.8	41.9	45.5	43.7
Ni	195.9	205.3	245.3	144.9	198.2	124.6	134	133	136	135	133
Cu	64.3	52.0	59.9	49.4	71.1	40.3	56.0	53.3	51.0	51.2	51.2
Zn	141.2	126.0	109.3	149.5	111.8	162.4	143.9	144.6	134.4	146.2	141.8
Ga	27.7	21.9	19.2	23.4	19.4	22.2	23.3	23.6	23.5	23.9	23.7
Rb	50.0	54.6	31.4	63.9	33.4	80.0	63.8	63.7	63.4	64.6	64.2
Sr	594	937	561	1076	534	1023	1068	1085	1071	1089	1087
Y	30.5	29.2	24.3	31.3	24.8	25.1	31.5	31.6	31.5	31.7	31.7
Zr	202	353	185	386	178	355	379	383	382	383	382
Nb	44.1	90.2	41.7	90.2	41.5	85.6	89.1	89.6	89.7	89.9	90.0
Mo	2.49	5.25	1.93	5.02	2.53	4.83	4.70	4.93	4.08	4.22	4.04
Cd	–	0.090	0.089	0.118	0.068	–	0.123	0.113	0.099	0.089	0.094
Sn	3.2	8.8	9.6	15.7	5.8	6.0	19.0	13.1	10.4	8.2	9.3
Sb	–	0.101	0.048	0.107	0.053	–	0.090	0.079	0.082	0.098	0.076
Cs	0.92	0.91	0.30	1.03	0.68	1.53	1.02	1.03	0.92	0.96	0.92
Ba	530.7	651.6	414.8	833.0	406.1	224.8	836.0	830	826	825	828
La	34.9	59.6	29.0	63.7	30.0	53.3	62.9	63.6	63.2	63.3	63.4
Ce	73.2	111.9	56.7	123.4	58.0	121.2	123	124	123	123	123
Pr	8.5	14.1	7.0	16.0	7.2	11.0	15.7	15.9	15.8	15.8	15.9
Nd	36.1	50.7	28.1	57.8	29.0	44.2	59.0	58.4	58.2	62.2	62.4
Sm	8.0	9.9	6.3	11.5	6.5	7.7	11.3	11.6	11.5	11.5	11.5
Eu	2.36	3.13	2.12	3.64	2.16	2.50	3.61	3.67	3.65	3.68	3.67
Tb	7.59	1.24	0.91	1.38	0.94	6.92	1.37	1.40	1.39	1.39	1.39
Gd	1.04	8.72	6.14	9.91	6.34	0.92	9.81	9.99	9.94	9.96	9.94
Dy	6.05	5.98	4.73	6.55	4.88	4.87	6.51	6.61	6.57	6.58	6.56
Ho	1.00	1.06	0.87	1.14	0.90	0.80	1.13	1.15	1.14	1.15	1.15
Er	2.61	2.52	2.16	2.66	2.22	1.96	2.64	2.69	2.67	2.68	2.69
Yb	1.76	1.80	1.60	1.89	1.67	1.43	1.85	1.88	1.86	1.86	1.88
Lu	0.266	0.246	0.222	0.252	0.229	0.205	0.249	0.254	0.253	0.254	0.253
Hf	5.38	7.21	4.22	7.98	4.08	9.34	7.90	7.98	7.96	7.99	7.94
Ta	2.35	5.24	2.47	5.27	2.48	4.38	5.39	5.42	5.24	5.40	5.34
Pb	2.52	5.39	3.17	5.36	3.20	5.22	5.34	5.52	5.41	5.36	5.46
Th	4.410	8.571	4.156	8.205	4.230	8.088	8.170	8.179	8.265	8.228	8.257
U	1.082	2.204	0.735	2.125	1.046	2.102	2.073	2.114	2.102	1.958	2.100
^{226}Ra (fg/g)	410.7	–	–	–	–	790.8	–	–	–	–	–
$^{87}Sr/^{86}Sr$	0.704153	0.703984	0.704042	0.703766	0.704111	0.703566	0.704026	0.704084	0.704153	0.704012	0.704082
$^{143}Nd/^{144}Nd$	0.512801	0.512802	0.512765	0.512800	0.512712	0.512766	0.512804	0.512813	0.512767	0.512794	0.512763
$(^{234}U/^{238}U)$	0.995	1.000	1.008	0.997	0.999	0.99	0.998	0.997	0.999	0.996	0.996
$(^{238}U/^{232}Th)$	0.744	0.780	0.537	0.786	0.750	0.79	0.770	0.784	0.772	0.722	0.771
$(^{230}Th/^{232}Th)$	0.828	0.881	0.840	0.897	0.841	0.90	0.896	0.895	0.898	0.895	0.896
$(^{226}Ra/^{230}Th)$	1.024	–	–	–	–	1.004	–	–	–	–	–

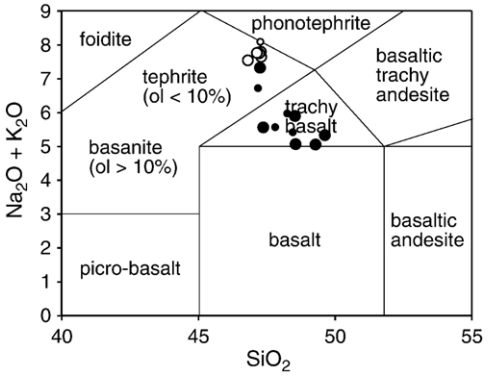

Fig. 3. Plot of total alkalis versus silica for samples from Mounts Gambier (filled circles) and Schank (open circles). Small symbols are supplementary data from Song (1994).

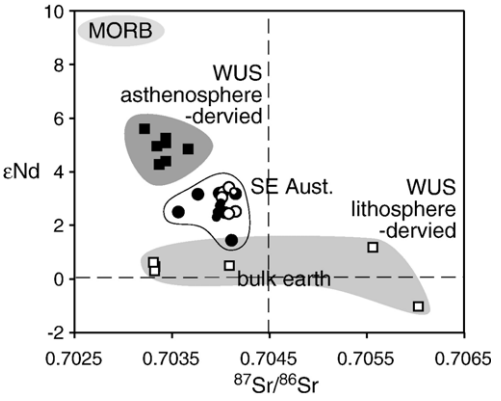

Fig. 5. εNd versus $^{87}Sr/^{86}Sr$ (symbols as in Fig. 3). Small symbols are supplementary data from Song (1994). Also plotted are samples inferred to have been derived from asthenospheric and lithospheric sources in the western U.S.A. (Asmerom and Edwards, 1995; Asmerom, 1999).

presented in Table 1 show that the samples are all relatively un-evolved basalts with SiO_2=46.8–49.6%, MgO=6.9–9.1%, Ni=133–245 ppm, Cr=140–297 ppm and Mg#=52–59. They are alkalic with Na_2O=3.6–4.8% and K_2O=1.5–3.0% (Fig. 3) and significantly enriched in incompatible trace elements and light rare earth elements (e.g. Rb=31–65 ppm, La=24–69 ppm, Yb=1.6–1.9 ppm) and the most mafic samples have primitive mantle-normalised incompatible trace element diagrams which are concave upward and relatively smooth (Fig. 4). In detail, many of the basalts have subtle U–K–Ti anomalies (see below). $^{87}Sr/^{86}Sr$ ranges from 0.7038 to 0.7042 and $^{143}Nd/^{144}Nd$ from 0.51271 to 0.51281 making these basalts distinct from mid-ocean ridge basalts (MORB) but similar to many OIB which cluster around the bulk Earth values (Fig. 5). On Fig. 5 they also plot between suites basalts from the western USA that have been inferred to have been derived from asthenospheric and lithospheric mantle sources. ($^{234}U/^{238}U$) ratios are all within error of secular equilibrium consistent with a lack of post-depositional alteration (Table 1). Since the age constraints suggest that all the volcanics at Mounts Gambier and Schank were erupted less than 5 kyr ago (Barbetti and Sheard, 1981; Blackburn et al., 1982), no age correction was applied to the U–Th disequilibria data. U and Th concentrations are relatively high (0.7 to 2.2 ppm and 4.2 to 8.6 ppm, respectively) and ($^{238}U/^{232}Th$) ranges from 0.54–0.79. ($^{230}Th/^{232}Th$) varies from 0.84 to 0.90 and all samples have ^{230}Th excesses with ($^{230}Th/^{238}U$)= 1.12 to 1.57 (Fig. 6). Samples GA1 and GA9 yielded measured ($^{226}Ra/^{230}Th$) ratios of 1.024 and 1.004, respectively. Thus, the former appears to have real ^{226}Ra–^{230}Th disequilibria whereas the latter is within

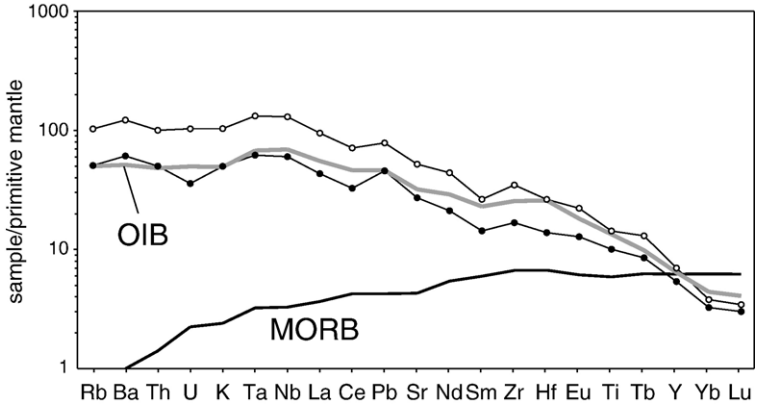

Fig. 4. Primitive mantle-normalised incompatible element diagram for high MgO samples (symbols as in Fig. 3).

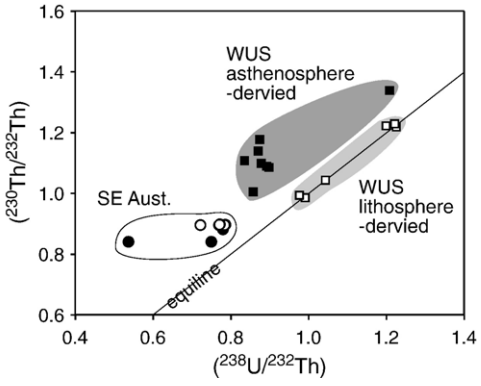

Fig. 6. U–Th equiline diagram for samples (symbols as in Fig. 3). Also plotted are samples inferred to have been derived from asthenospheric and lithospheric sources in the western U.S.A. (Asmerom and Edwards, 1995; Asmerom, 1999).

error (±1%) of secular equilibrium. However, the uncertainty in the age of the samples prevents calculation of erupted (^{226}Ra/^{230}Th) ratios.

6. Discussion and interpretation

It is not our primary objective here to investigate the cause of within-suite, fractionation-related geochemical variations of the basalts from Mounts Gambier and Schank, since this has been discussed in some detail elsewhere (Song, 1994; Demidjuk, 2005). Pertinent observations from those studies are the restricted range in the major and trace element chemistry which is consistent with modest degrees of fractionation of an assemblage composed of olivine and clinopyroxene. Least squares and coupled trace element modelling suggest that the extent of this fractional crystallisation may have ranged from 5 to ≤50% (Song, 1994; Demidjuk, 2005). Incompatible trace element patterns and Sr–Nd isotope data from these samples are very similar to many OIB (cf. Figs. 4 and 5). In principle, source regions bearing such signatures could be located either within the lithospheric mantle or within the convecting asthenosphere, potentially in a mantle plume but, as noted above, this has yet to be resolved for the Newer Volcanic Province (Paul et al., 2005).

6.1. Melting in static lithosphere or upwelling asthenosphere?

Previous studies (Frey et al., 1978; McDonough et al., 1985) have suggested that the Cones series alkali basalts reflect 3–6% partial melting of a garnet–lherzolite source region and rare earth element modelling is consistent with 2–8% residual garnet in their source region (Frey et al., 1978; Demidjuk, 2005). The lithospheric mantle beneath southeastern Australia is estimated to be ≤140 km thick (Kennett, 2003) and the garnet–spinel transition in fertile peridotite has been experimentally constrained to occur at ~90 km depth (Robinson and Wood, 1998). Therefore, it seems likely that the basalts from Mounts Gambier and Schank were derived either from the lower lithospheric mantle or else the asthenosphere, or a combination of both. Partial melting in static lithosphere is likely to occur via a process reasonably approximated by batch melting because the driving mechanism for melt segregation is negative buoyancy alone whereas in the asthenosphere this will be augmented by deformation and compaction. However, it is very difficult to produce significant U–Th disequilibria by such a process (see Elliott, 1997, for a discussion) because the partition coefficients (D) for U and Th are very similar (Blundy and Wood, 2003). In Fig. 7a and b we show the results of simple batch melting models that encompass appropriate degrees of melting and amounts of residual garnet. An extreme model, with 3% melting and 14% residual garnet, can produce about 10% ^{230}Th excess similar to those samples which have the smallest ^{230}Th excesses. However, five of the samples have ≥16% ^{230}Th excess which would require ≤ 1% melting and = 15% residual garnet which we consider unreasonable (cf. Frey et al., 1978).

Instead, the data from Mounts Gambier and Schank appear to require models which allow for ^{230}Th in-growth during melting and such models usually involve some form of dynamic melting in which the peridotite matrix is upwelling through the melting region (cf. Elliott, 1997). The disequilibria produced in such calculations is controlled by the melting rate and the residual porosity (ϕ) in the melting region. Unfortunately, the uncertainties in the age of the samples and the near equilibrium measured (^{226}Ra/^{230}Th) ratios preclude any rigorous constraint upon ϕ. However, U–Th disequilibria are more sensitive to melting (and thus inferred upwelling) rate than residual porosity which controls the disequilibria of highly incompatible elements like Ra (Bourdon and Sims, 2003). Thus, for ϕ we used a value of 0.1% which is at the lower end of values typically inferred from OIB's (e.g. Bourdon and Sims, 2003) but the exact choice of this parameter does not significantly alter the conclusions. Fig. 5c shows the results of one-dimensional, dynamic melting models (after Williams and Gill, 1989) which can simulate the data. We have assumed that melting occurs at depths greater than 140 km and chosen U and Th partition coefficients for garnet and clinopyroxene that are appropriate for this pressure (Table 2, Blundy and Wood, 2003). The models were also constrained to produce 200–400 m of melt thickness on the basis of the

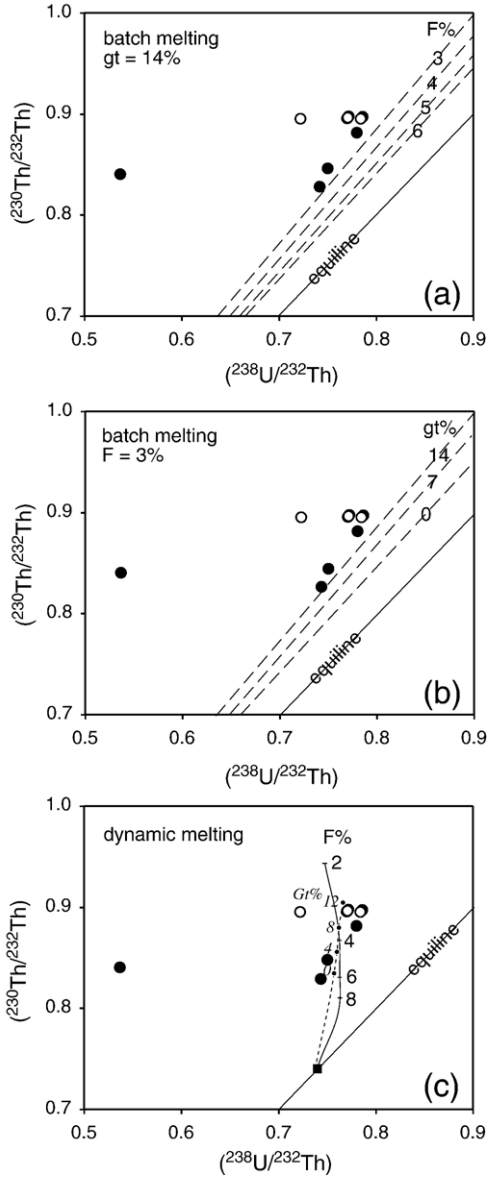

Fig. 7. U–Th equiline diagrams comparing data from Mounts Gambier and Schank (symbols as in Fig. 3) with (a) a batch melting model with a constant amount of residual garnet (14%) and variable degrees of melting, (b) a batch melting model with a constant degree of melting (3%) and varying amounts of residual garnet, and (c) a dynamic melting models based on the equations of Williams and Gill (1989): thin line assumes 6% residual garnet and 2–8% total melting (ticks along curve); dashed line assumes 4% total melting and 0–12% residual garnet (italics). All other model parameters given in Table 2.

likely thicknesses of basalt in the region. As discussed above, the basalts are relatively un-evolved and the entrainment of mantle xenoliths suggests rapid passage through the lithosphere and so it seems unlikely that there are large hidden volumes at depth. Adopting these constrains, appropriate degrees of partial melting (3–6%) in the presence of 6% residual garnet can reproduce the ^{230}Th excesses observed in all but one of the samples (Fig. 7c) if the melting region is upwelling at ~1.5 cm/yr (see Table 2) with a melt productivity range of 1–5%/kbar (cf. Asimow et al., 1997). The ^{230}Th excesses in the basalts are smaller than those commonly observed in many MORB and OIB (Bourdon et al., 2003) but this can be explained by the much shorter melting column (see Table 2). Varying the amount of residual garnet between 0 and 12% at a fixed 4% total melting produces very similar results to varying the overall extent of melting (see Fig. 7c). Thus, our new U–Th disequilibria data strongly suggest that the melting responsible for the basalts at erupted Mounts Gambier and Schank occurred in upwelling asthenopsheric mantle. This could, in principle, support models invoking the presence of a (mild) mantle plume beneath southeastern Australia (but see further discussion below). The anomalous sample GA-4 (see Fig. 7, Table 1) requires a source which had a lower initial U/Th ratio and either slower upwelling or a longer melting column to account for its larger observed ^{230}Th excess. Note that the transport of mantle xenoliths to the surface requires that, once segregated, the melts ascended rapidly.

It might be argued that the ^{230}Th excesses in the Mount Gambier and Schank basalts do not require active upwelling and simply reflect slow protracted melting of a static source since this could, in principle, still allow for ^{230}Th ingrowth during melting. However, melt production will be self-limiting in such a model because the solidus will rise as the fertility of the peridotite decreases due to melt extraction. In the western USA, Asmerom and co-workers (Asmerom and Edwards, 1995; Asmerom, 1999; Asmerom et al., 2000) have analysed U-series disequilibria in basalts which

Table 2
Modelling parameters

	Mode	D_U	D_{Th}
Olivine	52	6.00E−05	9.52E−06
Orthopyroxene	28	7.80E−03	3.00E−03
Clinopyroxene	20–6	8.70E−03	6.00E−03
Garnet	0–14	1.65E−02	3.30E−03
Dynamic melting model inupts:			
Melt column hight (km)		5	
Melt thickness (km)		0.2–0.4	
Residual porosity (ϕ)		0.001	
Melt density (ρ_m, kg/m^3)		2700	
Solid density (ρ_s, kg/m^3)		3300	
Upwelling rate (=W, cm/yr) [a]		1.5	
Melting rate (M, kg/m^3/yr)		3.96E−04	

Partition coefficients based on Blundy & Wood (2003).
[a] Calculated as (M×melt column height)/(ρ_s×melt%).

had previously been subdivided into asthenosphere- and lithosphere-derived on the basis of Nd isotopes and other data (e.g. Perry et al., 1987; Farmer, 2004). They showed that this distinction was also evident in U–Th disequilibria with the asthenosphere-derived basalts having significant ^{230}Th excesses, similar to those from Mounts Gambier and Schank, and the lithosphere-derived basalts being in secular equilibrium (Fig. 6). At the time, this distinction was interpreted to result largely from the presence or absence of residual garnet (which has $D_U/D_{Th}>1$) in the basalt source regions and so the presence or absence of ^{230}Th excess was essentially used as a novel form of geobarometer (Asmerom and Edwards, 1995; Asmerom, 1999; Asmerom et al., 2000). However, subsequent theoretical and experimental evidence has shown that D_U/D_{Th} in clinopyroxene also becomes >1 at pressures over 1 GPa (Landwehr et al., 2001) and so the effect of the presence or absence of residual garnet on the U–Th disequilibria of melts produced at depths greater than 35–50 km is likely to be much less than previously assumed. As illustrated in Fig. 7c, significant ^{230}Th excesses are produced by dynamic melting even when the amount of residual garnet is zero (see also Turner et al., 2000). Therefore, we suggest that the distinction between asthenosphere- and lithosphere-derived basalts on Fig. 6 reflects differences in the melting process; static batch melting in the lithosphere versus dynamic melting in an upwelling melting column in the asthenosphere. ^{231}Pa–^{235}U (and ^{226}Ra–^{230}Th) disequilibria will be less diagnostic because the bigger contrast between the parent and daughter nuclides of these pairs permit batch melting (as well as dynamic) models to create significant disequilibria (e.g. Asmerom et al., 2000).

6.2. Cause of melting beneath the continent

The thickness and volume of the Newer Volcanic Province are both significantly less than other intraplate basaltic provinces such as the Eastern Snake River Plain, which is volcanologically similar to the Newer Volcanics Province (Hare and Cas, 2005). Volcanism in the Eastern Snake River Plain is related to Basin and Range extension above the Yellowstone hotspot which has led to magma production through decompression melting within the plume. In southeastern Australia, there is no evidence for extension but U-series disequilibria data from the youngest basalts erupted at Mounts Gambier and Schank do provide evidence for mild upwelling. However, the estimated rate of upwelling (~1.5 cm/yr) is significantly less that that for even very mild plumes such as the Azores which is inferred to be upwelling at a rate of 3.5 cm/year due to a temperature ~70 °C above that of ambient mantle (Bourdon et al., 2005). If the plume hypothesis is adopted, then because buoyancy flux and upwelling rate are proportional to excess temperature, it is possible to estimate that the temperature of the mantle beneath southeastern Australia is likely to be no more than ~30 °C above that of ambient mantle. However, the lithosphere here is at least 100 km thick (Kennett, 2003) and at that depth the anhydrous peridotite solidus is about 1500 °C requiring an excess temperature similar to that inferred for the plume beneath Hawaii for melting to occur (e.g. McKenzie and Bickle, 1988).

Several factors suggest that upwelling beneath southeastern Australia is likely to have a very limited scope. Firstly, the region is currently in a state of tectonic compression (e.g. Sandiford et al., 2004) with neotectonic features across western Victoria and South Australia implying that this has been the case since at least 5 Myr ago (Sandiford, 2003), when the Newer Volcanic Province initiated. Deep-seated plumes like that beneath Hawaii are normally associated with extension in the overriding plate, because of the dynamic stress transferral from the flow as well as changes in potential energy induced by the compensation of plume related thermal buoyancy. Secondly, there is no apparent systematic spatial patterning in, or N–S elongation of, the Newer Volcanic Province consistent with absolute Australian plate motion (Price et al., 2003; Sutherland, 2003). In the ~5 Myr period of activity in the Newer Volcanic Province Australia has drifted north by more than 300 km, with significant differential motion across the mantle evidenced in the pronounced seismic anisotropy at sub-lithospheric depths (Debayle et al., 2005). Despite this, the N–S width of the province is typically less than 100 km, and much less than its ~400 km E–W extent. Thus, rather than being decoupled from plate motion, the space-time distribution of the Newer Volcanics suggests that the melting zone is somehow 'locked' into plate motion. Finally, while the volcanic province broadly correlates with a region of low-amplitude (order 100 m) uplift (Figs. 1 and 2), this uplift pattern defines a linear trend broadly oriented E–W, with an across strike wavelength (order 100 km) much smaller than expected from typical plume activity. Rather this topographic expression and distribution of volcanism suggests the upwelling is more likely a very localised phenomenon with a pronounced elongation more-or-less at right angles to plate motion. We believe that together these factors suggest that the mild upwelling evidenced by the ^{238}U–^{230}Th disequilibria must (1) relate to absolute plate motion and (2) be confined to the upper mantle.

Australia's absolute northward plate motion (~6.5 cm/yr) makes it the fastest moving of all the continents. Differential motion between the lithosphere and asthenosphere is implied by the unique (for sub-continental mantle) expression in seismic anisotropy. At depths of ~300 km beneath Australia the anisotropy is well aligned with absolute plate motion, whilst at shallow levels it shows variable alignment (Debayle et al., 2005; Heintz and Kennett, 2005). King and Anderson (1998) have shown that thermal contrasts associated with steps in lithospheric thickness will produce a pattern of small-scale circulation, that they term 'edge-driven' convection, that will be confined to the upper mantle above the transition zone. Such edge-driven convection is unsteady and sensitive to the thermal structure and relative motion of the overlying lithosphere. In particular, in the presence of such plate motion, edge-driven convection downstream of a lithospheric (shallowing) step produces a pattern of circulation confined to the upper few hundred kilometres of mantle, that travels with the overlying lithosphere, and is aligned with the trend of the step (Fig. 8a). King and Anderson's (1998) experiments produced upwelling located downstream approximately 150% of the step size, with flow rates of about 2 cm/yr.

A notable feature of Australian surface wave tomographic studies is a significant step in lithospheric structure (Kennett et al., 2004) loosely associated with the so-called "Tasman Line", corresponding to the transition between older Proterozoic and younger Phanerozoic lithosphere (Kennett et al., 2004). This is evident in a contrast in seismic velocities at depths between 125–225 km implying thicker mantle lithosphere to the north and west and thinner lithosphere to the south and east. Of particular note to our study is the transition in surface wave velocity anomalies at 125 km depth some 300–400 km north of Mount Gambier along a zone trending at ~80° E (Fig. 9). This apparent step in lithospheric structure lies at high angle to upper absolute plate motion, and therefore may help to stimulate an edge-driven upwelling in the downstream direction to the south (Fig. 8b). To test this we have adapted King and Anderson's (1998) modelling approach, with geometries and plate velocities appropriate to south-east Australia (Fig. 8), noting that in-as-much as we also use an isoviscous mantle (with a Rayleigh number of $\sim 10^6$), the results can at best only be considered indicative. We use a 100 km lithospheric step and a plate velocity of 6 cm/year, and employ a FEM algorithm to solve the momentum and energy balances for incompressible flow subject to the Boussinesq approximation with an imposed upstream and downstream flow to simulate a differential velocity between the base of an irregular thickness overriding plate and the base of the upper mantle some 500–600 kms deeper. In keeping with King and Anderson (1998), our modelling reveals a pattern of induced edge-driven circulation characterised by an unsteady downwelling immediately beneath the step with a complimentary upwelling attaining a maxima rate at distances between 100–500 kms further downstream (Fig. 8b–c). Modelled upwelling rates vary from up to 1.6 cm/yr at the 'base-step' depth to 0.8 cm/yr at the 'half-step' depth (Fig. 8c–d). The vigour of the upwelling oscillates on a period of several 10's of million years (Fig. 8d), partly stimulated by variations in the influx of thermal instabilities generated in the upstream, upper thermal boundary layer, and swept downstream into the trailing edge-driven downwelling by the motion of the overriding plate.

In view of these observations we postulate that upwelling associated with the South Australian basaltic volcanism may in fact represent an edge-driven convection mode induced by the rapid differential motion of variable thickness Australian lithosphere and the underlying asthenosphere, rather than a broad zone of deeply sourced upwelling. However, a notable feature of our modelling, and that of King and Anderson (1998), is the low velocities of such edge-driven upwelling. While the modelled velocities are comparable with the upwelling rates inferred from the ^{230}Th excesses, they are not capable of inducing melting of anhydrous peridotite (Bourdon et al., 2005). As such, edge-driven circulation can only provide a plausible mechanism for localising the Newer Volcanic province if the upwelling mantle is anomalously fertile comparable with, for example, metasomatised lithospheric mantle which has a solidus nearer 1200 °C at 100–140 km depth (Olafsson and Eggler, 1983). We suggest two possibilities could account for existence of unusually fertile mantle in the upwelling zone, namely: (a) the entrainment of hydrated, metasomatised lithospheric in the upstream flow, (b) the existence of a chemical heterogeneities in the upper mantle beneath eastern Australia related to the Mesozoic history of subduction. It remains an open question of whether the edge-driven convection is sufficiently vigorous to entrain chemically buoyant lithosphere mantle in sufficient quantities to significantly enhance mantle fertility, and not one that is well suited to analysis with isovisocus modelling approach here. In both cases an attraction of the model is that it can potentially reconcile the plume-like Sr–Nd isotopic characteristics of the volcanics (Fig. 5) with the preceding arguments for the absence of any plume. Numerous studies have established that the lithospheric mantle beneath

southeastern Australia is hydrated and has appropriate $^{87}Sr/^{86}Sr$ ~0.704–0.705 and $^{143}Nd/^{144}Nd$ ~0.5126–0.5129 similar to the volcanics (Griffin et al., 1988; O'Reilly and Griffin, 1988; Stolz and Davies, 1988; Powell et al., 2004).

The hypothesis that basaltic magmatism reflects a secondary convective mode localised downstream of a step in lithospheric thickness provides several potential further insights into the timing and pattern of the magmatism and associated responses. Firstly, the upwelling

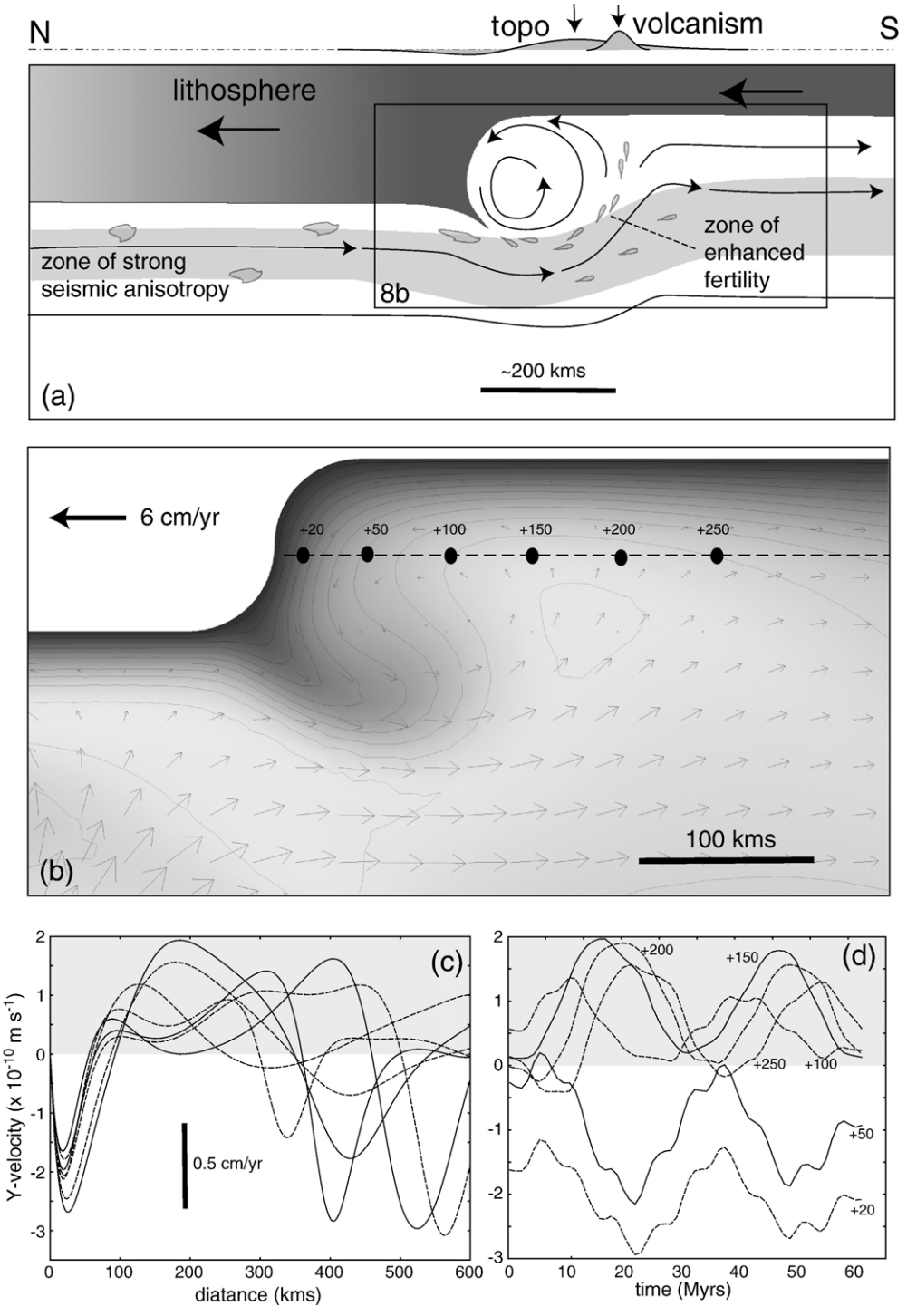

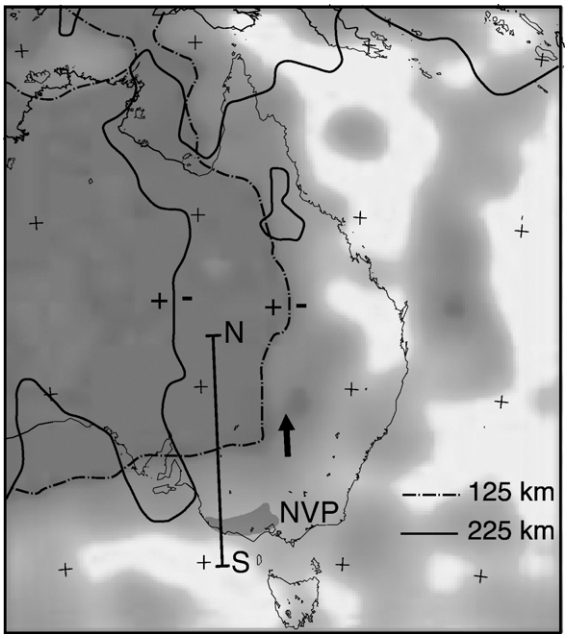

Fig. 9. Surface wave tomographic image of eastern Australia at depth of ~125 km (dark is fast, white is slow) from Kennett et al. (Olafsson and Eggler, 1983). The total amplitude of the anomaly is ±8% relative to ak135, with the neutral lines illustrated by the dashed line. The solid line shows the equivalent neural line at 225 km depth). Arrow shows absolute plate motion vector.

rates of ~1.5 cm/yr derived from ^{238}U–^{230}Th disequilibria imply a characteristic time scale for circulation on the order 10 Myrs, consistent with the insights gleaned from modelling illustrated on Fig. 8. This is consistent with the observations that the magmatic expression of mafic voclanism in south eastern Australia significantly post-dates the onset of fast plate motion of Australia which commenced about 43 Ma, some 38 Myr prior to the eruption of the oldest components of the Newer Volcanic Province. Also, flux rates and magmatic expressions of such forcing are likely to be unsteady on a period of order 10 Myrs. In the context of our discussion, an order 10 Myr period is implicated by the fact that the Newer Volcanic province is geographically correlated with older expressions of basaltic volcanism in Victoria dated to between 19 and 30 Ma (Price et al., 2003). It also conceivable that the ongoing uplift to the north of the Gambier volcanics extending back over the last 3–4 Myr, together with ongoing subsidence further north in the vicinity of the present day Murray River, may reflect the inherently unsteady nature of such flow. The second point concerns the distinctive offset of topographic uplift from the main axis of volcanism in the Newer Volcanic province (e.g. Fig. 1). Whereas the uplift reflects the primary response to the dynamic stresses generated by the upwelling flow and therefore should be localised above the fastest upwelling, melting will be sensitive to the distribution of fertility in the upwelling zone as well as upwelling rate. Consequently, these two different expressions of upwelling need not coincide. One reason that they may not is if, as argued above, fertility originates from the upstream realm, either by entrainment of lithosphere from the trailing edge of the lithospheric step or from incorporation of shallow, sub-lithospheric sources. The distribution of such anomalies is likely to be asymmetric, most strongly concentrated in the downstream part of the upwelling zone.

Finally, while many aspects of this pattern of small-scale circulation appear to provide a more attractive scenario for the Newer Volcanic province than a more deeply-sourced, plume-related upwelling, it does raise the obvious question of why such volcanism is then not more ubiquitous across Australia's southern margin, particularly in association with the transition from the thick cratonic lithosphere of the Gawler and Yilgarn Cratons to much thinner ocean lithosphere offshore South Australia and Western Australia, respectively. In as much as the upwelling rates and thermal anomalies associated with the edge-driven convection mode are insufficient to cause melting at sub-lithospheric depths, we have argued that enhancing fertility is fundamental. The absence of volcanism from much of Australia's southern margin suggests that the processes that enhance fertility provide the key to understanding the distribution of edge-driven convective magmatism, and these processes are the exceptional rather than the rule. The corollary is that the aerial distribution of the

Fig. 8. (a) Schematic interpretation of the small-scale, edge-driven convection (after King and Anderson, 1998) with application to the south-eastern Australian Newer Volcanic province, corresponding to the N–S section parallel to absolute plate motion shown in Fig. 9. Also shown is an indicative patterning of dynamic topography and volcanism associated with the edge-driven convection mode where melting reflects differential fertility associated with lithospheric entrainment. The axis of magmatism lies on the distal (downstream) side of the main axis of uplift. In the context of the Newer Volcanic province, the uplift axis corresponds to the Western Victorian Highland–Padthaway ridge axis (Fig. 2) while the subdued depression above the lithospheric edge corresponds to the Murray Basin. (b) Detail of isoviscous edge-driven convection model for a lithosphere moving at 6cm/yr to the left relative to the underlying asthenosphere. Arrows indicate velocity relative to the lithosphere, shading and contours (at 20 °C intervals) reflect temperature variations. (c) Modelled vertical velocity profiles at every ~10 Myr at the half step height (see dashed line in Fig. 8a). Distance is measured in kilometres downstream of the step. (d) temporal evolution of vertical velocity at a succession of points along the half step profile illustrated in Fig. 8b–c.

volcanics places constraints on the distribution of fertile lithospheric mantle.

6.3. A role for hydrous phases?

The role of volatiles is critical in the model presented above and so one test is whether there is geochemical evidence for the involvement of hydrous phases during melting. Hydrous phases preferentially incorporate Nb relative to U (e.g. LaTourrette et al., 1995; Ionov and Hofmann, 1995) and metasomatised lithospheric mantle xenoliths from southeastern Australia are characterised by the presence of amphibole±phlogopite which are strongly enriched in Nb (e.g. Griffin et al., 1988; O'Reilly and Griffin, 1988; Stolz and Davies, 1988; Powell et al., 2004). Thus, if the proposed secondary convection process lead to entrainment and melting of such material, the melts produced could be either enriched or depleted in Nb, relative to melts of anhydrous peridotite, depending on whether hydrous phases are residual or completely consumed, respectively. Fig. 10a shows that the basalts from Mounts Gambier and Schank have Nb/U ratios which are negatively correlated with U content and may extend to values which are both higher and lower than those typical of MORB and OIB. Lundstrom et al. (2003) observed a similar negative correlation between Nb/U and U amongst alkali basalts from the Canaries attributing the high Nb/U ratios to lithospheric contamination and the low Nb/U ratios to fractional crystallisation of amphibole±phlogopite. However, none of the basalts from Mounts Gambier and Schank contain hydrous phenocrysts. It is important to note that low Nb/U ratios are also a hallmark of the upper continental crust (e.g. Taylor and McLennan, 1985) and so the apparent trend towards low Nb/U ratios might instead be attributed to crustal contamination. However, those samples with the lowest Nb/U ratios do not systematically have the highest $^{87}Sr/^{86}Sr$ ratios (Fig. 10b) making such an explanation unlikely. Both amphibole and phlogopite are potassium-bearing minerals and on Fig. 10c we show that K/K*, calculated as $K_N/((U_N+Nb_N)/2)$ as a measure of the size of the K anomaly, also varies significantly in these rocks. Thus, there does appear to be reasonable geochemical evidence that hydrous phases played an important role during melting and, assuming an average Rb/Sr ratio of 0.02 for this component, it have formed from a component which separated from mantle with a MORB-like $^{87}Sr/^{86}Sr$ ratio of 0.7027 as long ago as 1 Ga.

One of the more intriguing observations in our dataset is that the trend towards low K/K* which we speculate reflects the interaction with melts formed in the presence of residual amphibole±phlogopite, is accompanied by decreasing $^{87}Sr/^{86}Sr$ (Fig. 10b, c). This is quite unusual and suggests involvement of mantle which was less radiogenic (i.e. more MORB-like) than the inferred, entrained lithospheric mantle yet which nonetheless contained hydrous phases. This might reflect hydration

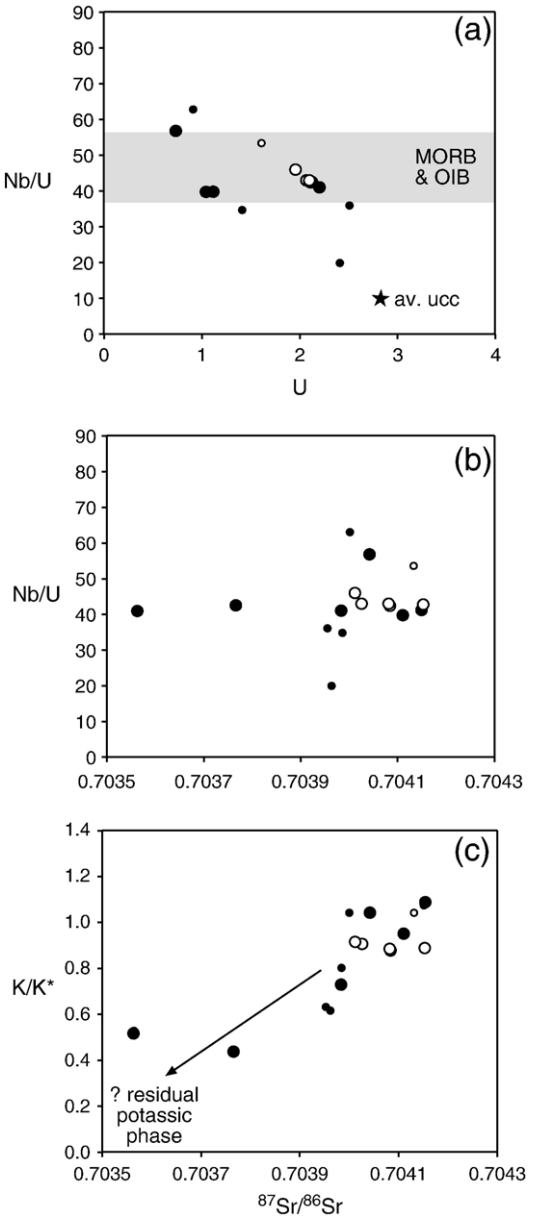

Fig. 10. (a) Nb/U versus U with range of MORB and OIB from Hofmann et al. (1986) and average upper continental crust (ucc) from Taylor and McLennan (Stolz and Davies, 1988). (b) Nb/U versus $^{87}Sr/^{86}Sr$. (c) K/K* versus $^{87}Sr/^{86}Sr$. Symbols as in Fig. 3; small symbols are supplementary data from (Song, 1994).

of portions of the asthenosphere that occurred during blending with metasomatised lithosphere entrained during the secondary convection process (cf. Fig. 8b). However, the southeastern Australian lithospheric mantle is complex and has evidently suffered multiple episodes of metasomatism variously involving silicate melt and hydrous/carbonate fluids (e.g. Powell et al., 2004 and references therein). Thus, an alternative explanation for the trend towards low K/K*, low $^{87}Sr/^{86}Sr$ component is one of mixing with partial melts during passage through the overlying metasomatised lithospheric mantle that was less ancient than, and which has not been sampled by, the xenolith suites.

7. Conclusions

In contrast to some, but not all, other continental basaltic provinces, a long-standing problem in understanding the Newer Volcanic Province of southeastern Australia has been to explain why mantle melting occurred in the absence of extension or any convincing evidence for the presence of a mantle plume beneath the region. Alkali basalts from southeastern South Australia have U–Th disequilibria which arguably require dynamic melting in upwelling mantle but the rate of upwelling is significantly less than that inferred for mantle plumes. We hypothesize that this mild upwelling takes the form of secondary convection cells driven by edge effects as the topography of the underside of the Australian plate migrates northward across the asthenosphere. In order to explain melting of mantle with has a normal potential temperature at 100–140 km depth, melting is linked to a significant contribution from hydrous mantle that is envisaged as resulting either from convective entrainment of lithosphere along the trailing edge of a lithospheric keel, or inherited variability in the asthenosphere. Geochemical evidence for this material is provided by enriched Sr–Nd isotopes in those basalts which have the largest ^{230}Th excesses. In our preferred model, the melts formed from this complex, blended mantle subsequently ascended through the overlying lithospheric mantle where they interacted with partial melts of amphibole±phlogopite peridotite leading to trends of decreasing K/K*. Interestingly, the effect of this interaction is to decrease $^{87}Sr/^{86}Sr$ which suggests that the portion of the lithospheric mantle where this took place underwent meatsomatism relatively recently. We speculate that other low volume but broadly distributed continental basaltic provinces which do not show a simple geographic age progression may result from similar secondary convection processes rather than demanding the presence of anomalously hot mantle.

Acknowledgements

We thank Scopenergy for financial support and Bob Dalgarno for field work assistance. Mark Lackie helped with the geophysical interpretation and Norm Pearson and David Bruce helped with the analytical work at Macquarie University and the University of Adelaide, respectively. Chris Hawkesworth provided useful suggestions and we are grateful to Tim Elliott and two anonymous reviewers for their helpful comments. This study used instrumentation funded by ARC LIEF and DEST Systemic Infrastructure Grants, Macquarie University and Industry. S.T. acknowledges the support of an ARC Federation Fellowship. This is GEMOC publication # 467.

References

Asimow, P.D., Hirschmann, M.M., Stolper, E.M., 1997. An analysis of variations in isentropic melt productivity. Philos. Trans. R. Soc. 355, 255–281.

Asmerom, Y., 1999. Th–U fractionation and mantle structure. Earth Planet. Sci. Lett. 166, 163–175.

Asmerom, Y., Edwards, R.L., 1995. U-series isotope evidence for the origin of continental basalts. Earth Planet. Sci. Lett. 134, 1–7.

Asmerom, Y., Cheng, H., Thomas, R., Hirschman, M., Edwards, R.L., 2000. Melting of the Earth's lithospheric mantle interred from protactinium–thorium–uranium isotopic data. Nature 406, 293–296.

Barbetti, M., Sheard, M.J., 1981. Palaeomagnetic results from Mounts Gambier and Schank, South Australia. J. Geol. Soc. Aust. 28, 385–394.

Belperio, A., Quaternary, in: J.F. Drexel, W.V. Preiss (Eds.), The Phanerozoic, The Geology of South Australia, vol. 2., South Australian Geological Survey Bulletin, 1995, vol. 54 pp. 219–280.

Blackburn, G., Allison, G.B., Leaney, F.W.J., 1982. Further evidence on the age of tuff at Mt Gambier, South Australia. Trans. R. Soc. S. Aust. 106, 163–167.

Blundy, J., Wood, B., 2003. Mineral-melt partitioning of Uranium, Thorium and their daughters. In: Bourdon, B., Henderson, G.M., Lundstrom, C., Turner, S.P. (Eds.), Uranium-series Geochemistry. Reviews in Mineralogy and Geochemistry, vol. 52. Geochemical Society-Mineralogical Society of America, Washington, pp. 59–123.

Bourdon, B., Sims, K.W.W., 2003. U-series constraints on intraplate basaltic magmatism. In: Bourdon, B., Henderson, G.M., Lundstrom, C.C., Turner, S.P. (Eds.), Uranium-series Geochemistry. Reviews in Mineralogy and Geochemistry, vol. 52. Geochemical Society-Mineralogical Society of America, Washington, pp. 215–254.

Bourdon, B., Henderson, G.M., Lundstrom, C.C., Turner, S.P. (Eds.), 2003. Uranium-series Geochemistry. Reviews in Mineralogy and Geochemistry, vol. 52. Geochemical Society-Mineralogical Society of America, Washington, p. 656.

Bourdon, B., Turner, S., Ribe, N.M., 2005. Partial melting and upwelling rates beneath the Azores from a U-series isotope perspective. Earth Planet. Sci. Lett. 239, 42–56.

Cheng, H., Edwards, R.L., Hoff, J., Gallup, C.D., Richards, D.A., Asmerom, Y., 2000. The half lives of uranium-234 and thorium-230. Chem. Geol. 169, 17–33.

Debayle, E., Kennett, B., Priestley, K., 2005. Global azimuthal seismic anisotropy: the unique plate-motion deformation of Australia. Nature 433, 509–512.

Demidjuk, Z., U-series insights into melting processes and magma evolution beneath the New Volcanic Province in South Australia. Hons. Thesis, Macquarie University, 2005, pp. 156.

Dosseto, A., Turner, S., Douglas, G.B., 2006. Uranium-series isotopes in colloids and sediments: time scale for sediment production and transport in the Murray–Darling river system. Earth Planet. Sci. Lett. 246, 418–431.

Eggins, S.M., Woodhead, J.D., Kinsley, L.P.J., Mortimer, G.E., Sylvester, P., McCulloch, M.T., Hergt, J.M., Handler, M.R., 1997. A simple method for the precise determination of =40 trace elements in geological samples by ICPMS using enriched isotope internal standardisation. Chem. Geol. 134, 311–326.

Elliott, T., 1997. Fractionation of U and Th during mantle melting; a reprise. Chem. Geol. 139, 165–183.

Farmer, G.L., 2004. Continental basaltic rocks. In: Rudnick, R.L. (Ed.), The Crust, Treatise on Geochemistry, vol. 3. Elsevier, Netherlands, pp. 85–121.

Foden, J., Song, S.H., Turner, S., Elburg, M., Smith, P.B., van der Steld, B., van Pengis, D., 2002. Geochemical evolution of lithospheric mantle beneath S.E. South Australia. Chem. Geol. 182, 663–695.

Frey, F.A., Green, D.H., Roy, S.D., 1978. Integrated models of basalt petrogenesis: a study of quartz tholeiites to olivine melilitites from south eastern Australia utilizing geochemical and experimental petrological data. J. Petrol. 19, 463–513.

Griffin, W.L., O'Reilly, S.Y., Stabel, A., 1988. Mantle metasomatism beneath western Victoria, Australia II: Isotope geochemistry of Cr-diopside lherzolites and Al-augite pyroxenites. Geochim. Cosmochim. Acta 52, 449–459.

Handler, M.R., Bennett, V.C., Esat, T.M., 1997. The persistence of off-cratonic lithospheric mantle: Os isotope systematics of variably metasomatised southeast Australian xenoliths. Earth Planet. Sci. Lett. 151, 61–75.

Hare, A.G., Cas, R.A.F., 2005. Volcanology and evolution of the Werribee Plains intraplate basaltic lava flow-field, Newer Volcanics Province, southeast Australia. Aust. J. Earth Sci. 52, 59–78.

Heintz, M., Kennett, B.L.N., 2005. Continental scale shear-wave splitting analysis: Investigation of seismic anisotropy underneath the Australian continent. Earth Planet. Sci. Lett. 236, 106–119.

Hofmann, A.W., Jochum, K.P., Seufert, M., White, W.M., 1986. Nb and Pb in oceanic basalts: new constraints on mantle evolution. Earth Planet. Sci. Lett. 79, 33–45.

Holdgate, G.R., Wallace, M.W., Gallagher, S.J., Witten, R.B., Stats, B., Wagstaff, B.E., 2006. Cenozoic fault control on 'deep lead' palaeoriver systems, Central Highlands, Victoria. Aust. J. Earth Sci. 53, 445–468.

Huang, Y., Hawkesworth, C., van Calsteren, P., Smith, I., Black, P., 1997. Melt generation models for the Auckland volcanic field, New Zealand: constraints from U–Th isotopes. Earth Planet. Sci. Lett. 149, 67–84.

Ionov, D.A., Hofmann, A.W., 1995. Nb–Ta-rich mantle amphiboles and micas: implications for subduction-related metasomatic trace element fractionations. Earth Planet. Sci. Lett. 131, 341–356.

Johnson, R.W., Knutson, J., Taylor, S.R., 1989. Intraplate volcanism in Eastern Australia and New Zealand. Cambridge University Press, Cambridge.

Kennett, B.L.N., 2003. Seismic structure in the mantle beneath Australia. In: Hillis, R.R., Müller, R.D. (Eds.), Evolution and dynamics of the Australian Plate. Geol. Soc. Aust. Spec. Publ., vol. 22, pp. 1–5.

Kennett, B.L.N., Fishwick, S., Reading, A.M., Rawlinson, N., 2004. Contrasts in mantle structure beneath Australia: relation to Tasman Lines? Aust. J. Earth Sci. 51, 563–569.

King, S.D., Anderson, D.L., 1998. Edge-driven convection. Earth Planet. Sci. Lett. 160, 289–296.

Landwehr, D., Blundy, J., Chamorro-Perez, E.M., Hill, E., Wood, B.J., 2001. U-series disequilibria generated by partial melting of spinel lherzolite. Earth Planet. Sci. Lett. 188, 329–348.

LaTourrette, T., Hervig, R.L., Holloway, J.R., 1995. Trace element partitioning between amphibole, phlogopite, and basanite melt. Earth Planet. Sci. Lett. 135, 13–30.

Lundstrom, C.C., Hoernle, K., Gill, J., 2003. U-series disequilibria in volcanic rocks from the Canary islands: Plume versus lithospheric melting. Geochim. Cosmochim. Acta 67, 4153–4177.

Mahoney, J.J., Coffin, M.F., 1997. Large igneous provinces: continental, oceanic and planetary flood volcanism. Geophysical Monograph, vol. 100. American Geophysical Union, Washington, DC, p. 438.

McBride, J.S., Lambert, D.D., Nicholls, I.A., Price, R.C., 2001. Osmium isotopic evidence for crust–mantle interaction in the genesis of continental intraplate basalts from the Newer Volcanics Province, Southeastern Australia. J. Petrol. 42, 1197–1218.

McDonough, W.F., McCulloch, M.T., 1987. The southeast Australian lithospheric mantle: isotopic and geochemical constraints on its growth and evolution. Earth Planet. Sci. Lett. 86, 327–340.

McDonough, W.F., McCulloch, M.T., Sun, S.-S., 1985. isotopic and geochemical systematics in Tertiary–Recent basalts from southeastern Australia and implications for the evolution of the sub-continental lithosphere. Geochim. Cosmochim. Acta 49, 2051–2067.

McKenzie, D.P., Bickle, M.J., 1988. The volume and composition of melt generated by extension of the lithosphere. J. Petrol. 29, 625–679.

Olafsson, M., Eggler, D.H., 1983. Phase relations of amphibole, amphibole-carbonate, and phlogopite-carbonate peridotite: petrologic constraints on the asthenosphere. Earth Planet. Sci. Lett. 64, 305–315.

O'Reilly, S.Y., Griffin, W.L., 1988. Mantle metasomatism beneath western Victoria, Australia I: Metasomatic processes in Cr-diopside lherzolites. Geochim. Cosmochim. Acta 52, 433–447.

Paul, B., Hergt, J.M., Woodhead, J.D., 2005. Mantle heterogeneity beneath the Cenozoic volcanic provinces of central Victoria inferred from trace-element and Sr, Nd, Pb and Hf isotope data. Aust. J. Earth Sci. 52, 243–260.

Perry, F., Baldridge, W., DePaolo, D., 1987. Role of asthenosphere and lithosphere in the genesis of Late Cenozoic basaltic rocks from the Rio Grande rift and adjacent regions of the southwestern United States. J. Geophys. Res. 92, 9193–9213.

Potts, P.J., Webb, P.C., Watson, J.S., 1984. Energy dispersive X-ray fluorescence analysis of silicate rocks for major and trace elements. X-Ray Spectrom. 13, 2–15.

Powell, W., Zhang, M., O'Reilly, S.Y., Tiepolo, M., 2004. Mantle amphibole trace-element and isotopic signatures trace metasomatic episodes in lithospheric mantle, western Victoria, Australia. Lithos 75, 141–171.

Price, R.C., Gray, C.M., Frey, F.A., 1997. Strontium isotopic and trace element heterogeneity in the plains of the Newer Volcanic province, Victoria. Geochim. Cosmochim. Acta 61, 171–192.

Price, R.C., Nichols, I.A., Gray, C.M., 2003. Cainozoic igneous activity, in: W.D. Birch (Ed.), Geology of Victoria. Geol. Soc. Aust. Spec. Publ. 23, 361–375.

Putrika, K., Johnson, M., Kinzler, R., Longhi, J., Walker, D., 1996. Thermobarometry of mafic igneous rocks based on clinopyroxene-liquid equilibria, 0–30 kbar. Contrib. Mineral. Petrol. 123, 92–108.

Reid, M., 1995. Processes of mantle enrichment and magmatic differentiation in the eastern Snake River Plain: Th isotopic evidence. Earth Planet. Sci. Lett. 131, 239–254.

Reid, M.R., Ramos, F.C., 1996. Chemical dynamics of enriched mantle in the southwestern united states: thorium isotope evidence. Earth Planet. Sci. Lett. 138, 67–81.

Robinson, J.A.C., Wood, B.J., 1998. The depth of the spinel to garnet transition at the peridotite solidus. Earth Planet. Sci. Lett. 164, 277–284.

Sandiford, M., 2003. Neotectonics of southeastern Australia: linking the Quaternary faulting record with seismicity and in situ stress. In: Hillis, R.R., Müller, R.D. (Eds.), Evolution and Dynamics of the Australian Plate. Geol. Soc. Aust. Spec. Publ., vol. 22, pp. 101–113.

Sandiford, M., Wallace, M., Coblentz, D., 2004. Origin of the in situ stress field in southeastern Australia. Basin Res. 16, 325–338.

Sheard, M.J., 1978. Geological history of the Mount Gambier volcanic complex, southeast South Australia. Trans. R. Soc. S. Aust. 102, 125–139.

Sheard, M.J., Quaternary volcanic activity and volcanic hazards. in: J.F. Drexel, W.V. Preiss (Eds.), The Phanerozoic, The Geology of South Australia, vol. 2., South Australian Geological Survey Bulletin, 1995, vol. 54, pp. 264–268.

Song, S.H., Geochemical evolution of Phanerozoic lithospheric mantle beneath S.E. South Australia, PhD thesis, University of Adelaide, 1994, pp. 328.

Stolz, A.J., Davies, G.R., 1988. Chemical and isotopic evidence from spinel lherzoilite xenoliths for episodic metasomatism of the upper mantle beneath southeastern Australia. J. Petrol. Spec. Vol., pp. 303–330.

Sutherland, F.L., 2003. Boomerang migratory intraplate Cenozoic volcanism, eastern Australia rift margins and the Indo-Pacific mantle boundary. In: Hillis, R.R., Müller, R.D. (Eds.), Evolution and Dynamics of the Australian Plate. Geol. Soc. Aust. Spec. Publ., vol. 22, pp. 203–221.

Taylor, S.R., McLennan, S.M., 1985. The Continental Crust: Its Composition and Evolution. Blackwell Scientific, Oxford.

Teasdale, J., 2004. First-pass geological evaluation of Otway Basin Geothermal Energy Potential. FrOG Tech Project Code: SE501.

Turner, S., Blundy, J., Wood, B., Hole, M., 2000. Large ^{230}Th-excesses in basalts produced by partial melting of spinel lherzolite. Chem. Geol. 162, 127–136.

Wallace, M., Dickinson, J.A., Moore, D., Sandiford, M., 2005. Late Neogene strandlines of Southern Victoria: A unique record of eustasy and tectonics in southeast Australia. Aust. J. Earth Sci. 52, 277–295.

Wallace, M.W., Sandiford, M., Miranda, J., Holdgate, G.R., McLaren, S.N., Gallagher, S.J. , DeDeckker, P., in press. The formation of a giant Plio-Pliocene lake and the origin of the Murray River, southeastern Australia, Aust. J. Earth Sci.

Williams, R.W., Gill, J.B., 1989. Effects of partial melting on the uranium decay series. Geochim. Cosmochim. Acta 53, 1607–1619.

Zhang, M., Stephenson, P.J., O'Reilly, S.Y., McCulloch, M.T., Norman, M., 2001. Petrogenesis and geodynamic implications of Late Cenozoic basalts in North Queensland, Australia: trace element and Sr–Nd–Pb isotope evidence. J. Petrol. 42, 685–719.